ORIGINAL PAPER

Unplanned islanding detection of renewable energy sources using sequence impedance with zero NDZ

Indradeo Pratap Bharti[1] · Navneet Kumar Singh[1] · Om Hari Gupta[2] · Asheesh Kumar Singh[1]

Abstract

Unintentional islanding, defined as the inadvertent separation of distributed generators from the main grid, is a significant issue for wind power and synchronous-based microgrid. Islanding events must be detected to ensure safety and protect utility workers and equipment. The improper detection islanding may lead to power quality degradation, grid protection interference, and out-of-phase reclosing. To overcome these issues, researchers developed the islanding detection technique. This paper proposes a method, for accurately discerning between instances of islanding and those that are not islanding-related events, that employs two new criteria: (1) superimposed positive sequence impedance (SPSI) and (2) superimposed negative sequence impedance (SNSI). The islanding detection indices (IDI_1 and IDI_2) are calculated using the SPSI and SNSI. If the values of IDI_1 and IDI_2 exceed a predefined threshold, islanding is detected. The performance of the proposed approach is tested using the MATLAB/Simulink platform. The simulation results show that the proposed technique detects islanding in 20 ms at nearly zero power mismatch and under balanced conditions. Therefore, it limits unwanted tripping caused by various types of non-islanding events. The proposed technique is compared with existing schemes to demonstrate its superiority.

Keywords Synchronous generator-based microgrid · Islanding scheme · Superimposed of impedance · NDZ

Abbreviations

THD	Total harmonic distortion
ROCONSVAC	Rate of change of negative sequence voltage and current
SSSG	Small-scale synchronous generator
ROCOV	Rate of change of voltage
ROCOF	Rate of change of frequency
DG	Distributed generation
IEs	Islanding events
NIEs	Non-islanding events
FHO	Forced Helmholtz oscillator
MPPT	Maximum power point tracking
PAOPSV	Phase angle of positive sequence voltage
LSTM	Long short-term memory
IM	Impedance measurement
PIIS	Parallel inductive impedance switching
ROCOP-TV	Rate of change of power terminal voltage

✉ Indradeo Pratap Bharti
  indradeo.2019ree12@mnnit.ac.in

1 MNNIT Allahabad, Prayagraj, India

2 NIT Jamshedpur, Jamshedpur, India

1 Introduction

1.1 Motivation

In recent years, distributed energy sources like solar, wind, and small hydropower have been heavily integrated into the system for a variety of reasons, including increased power supply reliability and resilience, minimized power outages, avoidance of temporary interruption of critical loads, and reduction of environmental issues. When the penetration of microgrids into the power grid is observed, some technical challenges arise, such as the coordination of multiple generations, the sensitivity of protection schemes, and islanding detection and control. Islanding is one of the most serious risks associated with microgrids. There are two types of islanding: intentional and unintentional islanding. Intentional islanding serves for system maintenance and protection. Unintentional islanding conditions need to be quickly identified to take the necessary steps to maintain the safe operation of the network. The IEEE 1547 standard highlights how important it is to identify an islanding situation and separate the microgrid from the utility grid within 2 s [1].

1.2 Literature review

Several islanding detection algorithms have been presented in the literature over the last two decades by researchers and industry. Select the most appropriate islanding scheme for the converter and synchronous-based microgrid because the dynamic behavior of the synchronous-based microgrid is different from the converter-based microgrid after the islanding occurrence. The islanding techniques are classified as local and remote [2–4]. The local technique operated on the microgrid side. There are two types of local methods: active and passive. The passive scheme is affected by changes in parameters such as frequency, voltage, current, and THD. Passive method vulnerability is that choosing a threshold is challenging, and the non-detection zone (NDZ) is large. It includes the ROCONSVAC [5], change in apparent power [6], and the phase angle between negative sequence voltage and current [7]. Furthermore, intelligent-based passive islanding techniques have been proposed, which combine decision trees and data-mining models. In terms of reliability, training time requirements, and handling large data sets, decision trees outperform other data-mining algorithms such as artificial neural networks, support vector machines, and k-nearest neighbors. In a distribution system, decision tree regression is used to locate faults by combining the features of the discrete Fourier transform (DFT) and the discrete wavelet transform. Active islanding algorithms are based on injecting a small perturbance signal into the control network [8]. Numerous active schemes exist, including open-close of the SSSG circuit breaker [9], capacitor switching [10], and injected into the SSSG active/reactive power control loops [11]. It has a smaller NDZ than passive techniques. Active techniques degrade power quality. The drawbacks of passive and active strategies will be overcome by the use of hybrid techniques. Normally, the hybrid approaches are a combination of passive and active [12]. A few examples of hybrid techniques are fuzzy classifier and reactive power [13], rate of change of frequency and reactive power insert, and ROCOV and ROCOF [14, 15]. The remote technique is operated when information sends between the utility grid and distributed generation through the communication channel. The remote schemes operated on the utility grid side [16]. Remote techniques do not have a non-detection zone. These techniques are more accurate and reliable than local islanding methods, However, their utilization is extremely expensive due to the requirement of costly communications signals between the power system network.

1.3 Contributions

The literature survey above indicates that active techniques degrade power quality while remote schemes are more expensive. It is found that passive techniques fail to detect islanding at zero power mismatch. This article proposes a novel mixed islanding detection scheme based on an integrated superimposed sequence impedance. The mixed islanding technique provides a better response in all islanding and non-islanding environments. The proposed technique has been tested on synchronous and wind turbine-based DG microgrids. The following are the benefits of the suggested mixed detection method:

- This method is more effective than the other techniques.
- The suggested scheme quickly and accurately detected islanding at zero power mismatch.
- It performs well in NIEs, such as nonlinear loads and low fault resistance values.
- The scheme detects islanding in 20 ms.
- It is easy to implement at a low cost.
- The proposed method is tested for a converter and synchronous machine-based distributed generators.
- No issue with power quality.

The layout of this article is organized into sections: Sect. 2 describes the proposed scheme. Section 3 studies the test system and threshold setting. Section 4 is the test simulation and outcomes. Section 5 contained a comparison analysis and discussion. The conclusion of this paper is presented in Sect. 6.

2 The proposed methodology based on SPSI and SNSI

2.1 Mathematical calculation of sequence component

Figure 1 demonstrates step by step flow diagram of the proposed methodology. At first, the three-phase voltage and current signal are acquired at the PCC point. The voltage and current samples are collected over a one-cycle period at a sampling frequency of 1.2 kHz, and the system operates at a fundamental frequency of 60 Hz. The samples of voltage and current signals contain large harmonics. It is removed when passing through recursive DFT.

Let $y(t)$ be the input signal that operates at the system frequency f_0, whereas $N f_0$ is a sampling frequency and ϕ be phase angle in radians. To compute the phasor and magnitude of (1) using recursive DFT [17, 18].

$$y(t) = y_m Cos(2\pi f_0 t + \phi) \tag{1}$$

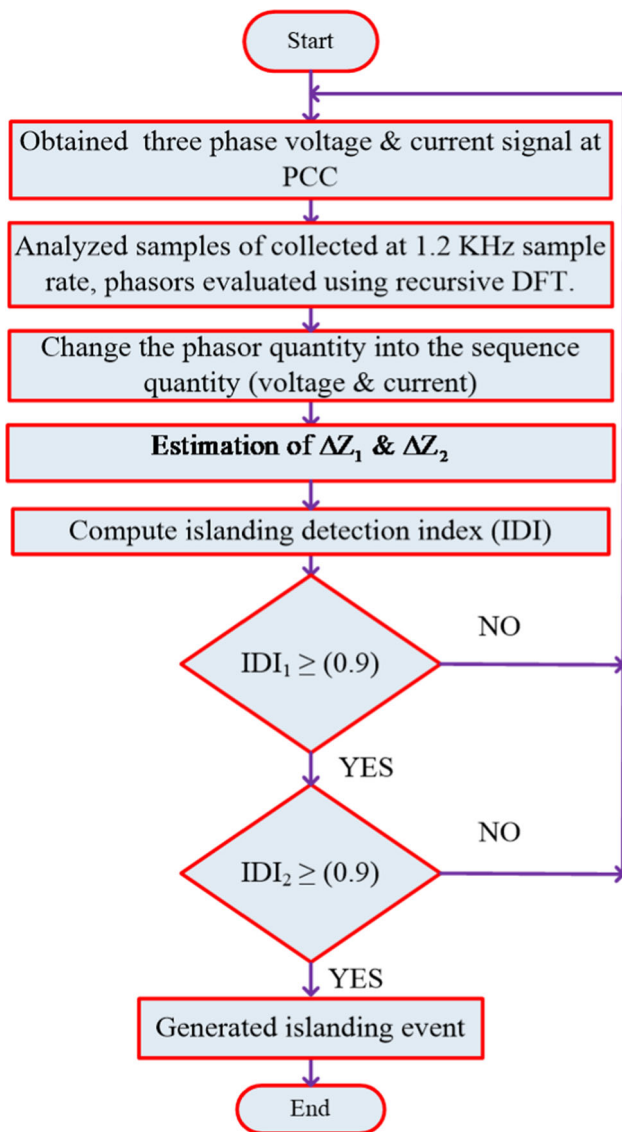where N is the input data sample y_n : $\{n = 0, 1, 2, ... N - 1\}$ given in (2). And sampling angle

Fig. 1 Flow diagram of the islanding detection method

$\theta = 2\pi/N$.

$$y_n = Y_m Cos(n\theta + \phi) \tag{2}$$

$$y_c^{N-1} = \frac{\sqrt{2}}{N} \sum_{n=0}^{N-1} y_n \cos(n\theta) \tag{3}$$

$$y_c^{N-1} = \frac{X_m}{\sqrt{2}} \cos\phi \tag{4}$$

Only the cosine $\cos(2n\theta)$ term is present in the above Eq. (4). The sine sum is estimated in the same way:

$$Y_s^{N-1} = \frac{\sqrt{2}}{N} \sum_{n=0}^{N-1} y_n \sin(n\theta) \tag{5}$$

$$Y_s^{N-1} = -\frac{y_m}{\sqrt{2}} \sin\phi \tag{6}$$

The phasor Y^{N-1} is represented by

$$Y^{N-1} = Y_c^{N-1} - jY_s^{N-1}$$

where $a = Y_c^{N-1}$ and $b = Y_s^{N-1}$ is the real and imaginary coefficients of the input signal, respectively. The above equation calculates the input signal's magnitude and phase angle using recursive DFT.

$$\left|Y^{N-1}\right| = \sqrt{a^2 + b^2} \text{ and } \theta = \tan^{-1}\left(\frac{b}{a}\right)$$

The three-phase voltage $(V_\alpha, V_\beta \text{ and } V_\gamma)$ and current $(I_\alpha, I_\beta \text{ and } I_\gamma)$ are estimated from recursive DFT as explained above. The voltage $(V_0, V_1 \text{ and } V_2)$ and current $(I_0, I_1 \text{ and } I_2)$ sequence components are acquired from the fundamental waveforms of three-phase voltage and current. Equations (7) and (8) express the connection between the phase and sequence of voltage and current.

$$\begin{bmatrix} V_0 \\ V_1 \\ V_2 \end{bmatrix} = \frac{1}{3} \times \begin{bmatrix} 1 & 1 & 1 \\ 1 & k & k^2 \\ 1 & k^2 & k \end{bmatrix} \times \begin{bmatrix} V_\alpha \\ V_\beta \\ V_\gamma \end{bmatrix} \tag{7}$$

$$\begin{bmatrix} I_0 \\ I_1 \\ I_2 \end{bmatrix} = \frac{1}{3} \times \begin{bmatrix} 1 & 1 & 1 \\ 1 & k & k^2 \\ 1 & k^2 & k \end{bmatrix} \times \begin{bmatrix} I_\alpha \\ I_\beta \\ I_\gamma \end{bmatrix} \tag{8}$$

where $k = 1\angle 120°$ is the complex operator.

2.2 Computation of positive and negative sequence impedances

If the microgrid network is operated under abnormal conditions, the voltage and current sequence components will change. Therefore, the impedances of the positive and negative sequences vary. From Eqs. (7) and (8), positive and negative sequences of voltage and current are expressed in Eqs. (9), (10), (11), and (12):

Where V_α, V_β, and V_γ are the three-phase voltage signal and can be written as phasor form $V_\alpha \angle \theta_\alpha$, $V_\beta \angle \theta_\beta$ and $V_\gamma \angle \theta_\gamma$, respectively. Similarly I_α, I_β and I_γ are a three-phase current signal that can be written as phasor form $I_\alpha \angle \theta_\alpha$, $I_\beta \angle \theta_\beta$ and $I_\gamma \angle \theta_\gamma$, respectively.

$$V_1 = \frac{1}{3}\big(V_\alpha \angle \theta_\alpha + V_\beta \angle (\theta_\beta + 120) + V_\gamma \angle (\theta_\gamma + 240)\big) \tag{9}$$

$$I_1 = \frac{1}{3}\big(I_\alpha \angle \theta_\alpha + I_\beta \angle (\theta_\beta + 120) + I_\gamma \angle (\theta_\gamma + 240)\big) \tag{10}$$
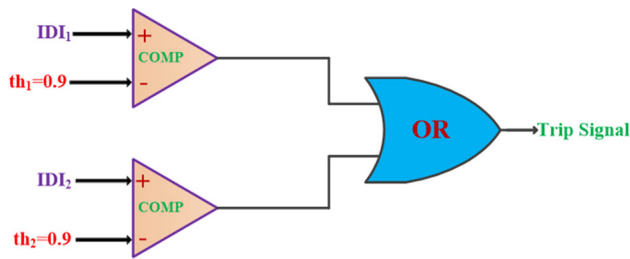
Fig. 2 Logic diagram of the proposed algorithm

$$V_2 = \frac{1}{3}\left(V_\alpha \angle \theta_\alpha + V_\beta \angle (\theta_\beta + 240) + V_\gamma \angle (\theta_\gamma + 120)\right) \quad (11)$$

$$I_2 = \frac{1}{3}\left(I_\alpha \angle \theta_\alpha + I_\beta \angle (\theta_\beta + 240) + I_\gamma \angle (\theta_\gamma + 120)\right) \quad (12)$$

Positive and negative sequence impedance can be calculated using Eqs. (9), (10), (11), and (12).

$$Z_1 = \frac{V_1}{I_1} \quad (13)$$

$$Z_2 = \frac{V_2}{I_2} \quad (14)$$

2.3 Estimate of superimposed positive and negative sequence impedances (SPSI and SNSI)

When an islanding or non-islanding event occurs, the superimposed positive and negative impedance is affected. It is referred to as the difference between the post-event and pre-event elements of positive and negative sequence impedance. SPSI and SNSI are computed using Eqs. (15) and (16)

$$\Delta Z_1 = \left|Z_{1pos}\right| - \left|Z_{1pre}\right| \quad (15)$$

$$\Delta Z_2 = \left|Z_{2pos}\right| - \left|Z_{2pre}\right| \quad (16)$$

2.4 Islanding detection index (IDI)

The absolute outputs of the SPSI and SNSI are used to calculate IDI$_1$ and IDI$_2$ (absolute means of ΔZ_1 and ΔZ_2) as shown in (17) and (18), respectively.

$$IDI1 = \frac{1}{T}\int_{t-T}^{t} |\Delta Z_1(t)|dt \quad (17)$$

$$IDI2 = \frac{1}{T}\int_{t-T}^{t} |\Delta Z_2(t)|dt \quad (18)$$

T in (17) and (18) shows the fundamental period of the system; t in the second is the instantaneous time. The IDI$_1$ and IDI$_2$ are compared with threshold th1 and th2 using a comparator (COMP) as shown in Fig. 2. When IDI$_1$ is greater than th1, logic is '1'; otherwise, logic is '0.' Similarly, if IDI$_2$ is greater than th2, the logic returns '1' otherwise '0.' Whenever at least one of them is '1' otherwise, its value is '0'. If logic '1' appears in the trip signal, it indicates islanding events and if logic '0' appears, it indicates non-islanding events.

3 Test system

Figure 3 represents the multi-bus validation test network operating at (25 kV, 60 Hz). Table 1 lists all the parameters of the distributed test network. There are two distributed

Fig. 3 Distributed test network under study

Table 1 The test Simulink model parameters

System components	Types	System index
Utility grid	Swing	1000 MVA, 120 kV, 60 Hz,
Grid transformer	Step down	120/25 kV, 47MVA, 60 Hz
DFIG transformer	Step up	575/25 kV, 10.5MVA, 60 Hz
Synchronous generator (DG)	PV	3.5 MVA, $V = 25$ kV, 60 Hz
Three-phase parallel RLC load	Z	$V = 25$ kV, 60 Hz, $P = 11.5$ MW, $Q = 1$ MVA
DFIG generator	PV	575 V, 9 MVA, 60 Hz
Distributed line variables:		
	π	$R_1 = 0.1153$ Ω/km, $R_0 = 0.413$ Ω/km, $X_1 = 1.05$mH/km, $X_1 = 3.32$mH/km, $C_1 = 11.33$nF/km, $C_0 = 5.01$nF/km
Length of line		20 km, 1 km
Asynchronous motor	Z	230 HP, $V = 25$ kV, 60 Hz

generators in the plant: a 9 MW wind farm and another 3.5 MW synchronous distributed generator integrated with the main grid of 1000MVA, 120 kV, and 60 Hz. The distribution network has evaluated various tests of islanding and non-islanding events with different sizes of DG at multiple buses.

3.1 Selection of threshold

Several factors affect threshold setting, including sampling interval, rating of distribution generators, system parameters, and network topology. Therefore, an optimal threshold value has been selected. In both islanding and non-islanding scenarios, the maximum magnitude of the IDI1 and IDI1 is calculated for selecting the threshold value, as illustrated in Table 2. The maximum magnitudes of IDI1 and IDI2 for a non-islanding event are 0.80 and 0.80, respectively. The minimum values of IDI_1 and IDI_2 for an islanding event are 1.3 and 2.8, respectively. The safety margin considered in this case is 0.1. To discriminate between IEs and NIEs perfectly, the value of the threshold (th1 and th2) is set to 0.9.

Threshold value = (The maximum value of the islanding detection index (IDI) in a non-islanding event + safety margin).

4 Simulation test results

Figure 2 illustrates a single-line diagram of the distributed network study. The various cases tested on the multi-bus network are classified as follows: The IEs at different active and reactive power (high, low, and zero) mismatch. NIEs include load, capacitor, fault, motor switching, voltage sag, and swell.

4.1 Islanding condition

When the microgrid is completely disconnected from the power grid and operates in stand-alone mode, it continuously supplies power to a local load. This event has an impact on the DG's voltage and frequency.

4.1.1 Islanding at different power mismatches

In most cases, hybrid methods are unable to detect islanding at low or zero power mismatches. This section evaluates the performance of the proposed scheme under various active and reactive power mismatches (0%, 25%, 75%) between distributed generation units and load demands. From Fig. 4a–b, the maximum magnitude of the islanding detection index (IDI_1 and IDI_2) at various power mismatches exceeds the predefined threshold (0.9). Islanding began at $t = 2$ s in this event. However, the proposed algorithm detects islanding at $t = 2.02$ s, as shown in Fig. 4c. The islanding detection time is 20 ms. According to the above discussion, the proposed mixed technique is more effective at zero power mismatch.

4.2 Non-islanding condition

The collaboration of the microgrid grid with the utility grid is known as grid-connected mode. The following are examples of non-islanding events (NIEs): load, capacitor, motor, and nonlinear load switching.

4.2.1 Impact of load switching

In this event, a load with a capacity of 4.5 MW and 1.2 MVAR is switched in the distribution test network at $t = 2$ s. To evaluate the performance of the mixed detection methodology for load switching. According to Fig. 5a–b, the response of the islanding detection index (IDI_1 and IDI_2) in both cases is less than the threshold value (0.9). Hence, the suggested technique remains stable when encountering load switching, without generating a trip signal, as illustrated in Fig. 5c.

4.2.2 Effect of capacitor switching

Parallel-connected capacitors are employed within the power system to enhance power factor and address voltage sags. In order to assess the efficiency of the suggested approach, an

Table 2 The maximum value of the islanding detection index (IDI) for various IEs and NIEs

Events		Maximum value IDI$_1$	Maximum value IDI$_2$	Number of test cases
Non-islanding events	Load switching	0.66	0.36	35
	Capacitor switching	0.41	0.47	25
	Nonlinear load switching	0.15	0.29	20
	Motor switching	0.60	0.65	30
	Single pole trip	0.67	0.79	10
	Voltage Sag	0.57	0.29	20
	Voltage swell	0.80	0.56	
	LLLG fault	0.78	0.80	80
	LLL fault	0.71	0.76	
	LLG fault	0.58	0.63	
	LL fault	0.55	0.59	
	LG fault	0.61	0.63	
Islanding events	Zero power mismatch	3.36	9.95	150
	Large power mismatch	4.4	10.1	

abrupt alteration in capacitive load, rated at 4.5 MVAR, is introduced at $t = 2$ s. From Fig. 6a–b, the magnitude of the islanding detection index (IDI$_1$ and IDI$_2$) in both cases is less than the predefined threshold value (0.9). Therefore, it does not initiate the trip signal as depicted in Fig. 6c. Hence, the proposed algorithm remains stable during abrupt changes in capacitive load.

4.2.3 Effect of motor switching

The electrical characteristics of the power system undergo modifications while switching the motor, during both connection and disconnection phases. These changes could potentially lead to disruptions in the anti-islanding protection of the DG system. To evaluate the performance of the proposed scheme, a 230HP motor load is switched in the test network at $t = 2$ s. In both cases, the values of the islanding detection index (IDI$_1$ and IDI$_2$) are less than the threshold value (0.9), as shown in Fig. 7a–b. Consequently, the proposed technique fails to detect islanding, and the initiated trip signal is zero, as shown in Fig. 7c. According to the above discussion, the proposed method remains stable during abrupt changes in motor load.

4.2.4 Effect of fault switching

To investigate the effectiveness of the mixed technique. However, various faults occurred in the test network. The different types of faults are given below:

- Symmetrical fault (LLLG, LLL)
- Asymmetrical fault (LG, LL, LLG)

A fault resistance of $0.01\,\Omega$ is switched in the distribution test network at $t = 2$ s. From Fig. 8a–b, the magnitude of the islanding detection index (IDI$_1$ and IDI$_2$) for symmetrical and asymmetrical fault is less than the threshold value of 0.9. In this case, the proposed approach does not detect islanding. Therefore, the algorithm does not generate the trip signal as shown in Fig. 8c.

4.2.5 Effect of nonlinear switching

In this section, a three-phase nonlinear diode rectifier load with a rating of 0.9 MW is switched in the multi-bus network at $t = 2$ s. From Fig. 9a–b, the response of the islanding detection index (IDI$_1$ and IDI$_2$) values in both cases is below a predefined threshold (0.9). Therefore, the proposed methodology does not detect it as islanding, and the system remains stable. The proposed method does not generate a trip signal as shown in Fig. 9c.

4.2.6 Effect of power quality disturbance

To evaluate the performance of the proposed scheme for power quality issues. A heavy load with capacity (22.5 MW and 3.4 MVAR) is injected into the test network at $t = 2$ s. In this case, the voltage drop is less than the normal voltage and is referred to as voltage sag. The response of this
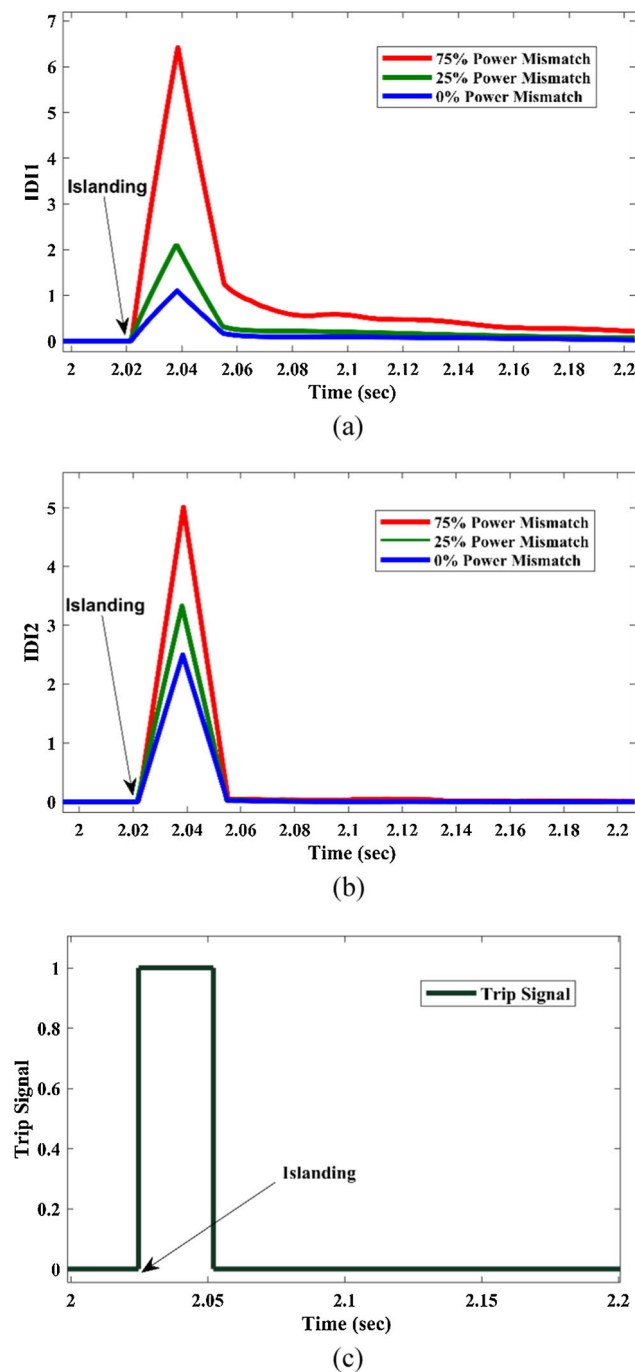
Fig. 4 Power mismatch Islanding detection condition **a** IDI_1 versus time **b** IDI_2 versus time **c** trip signal versus time
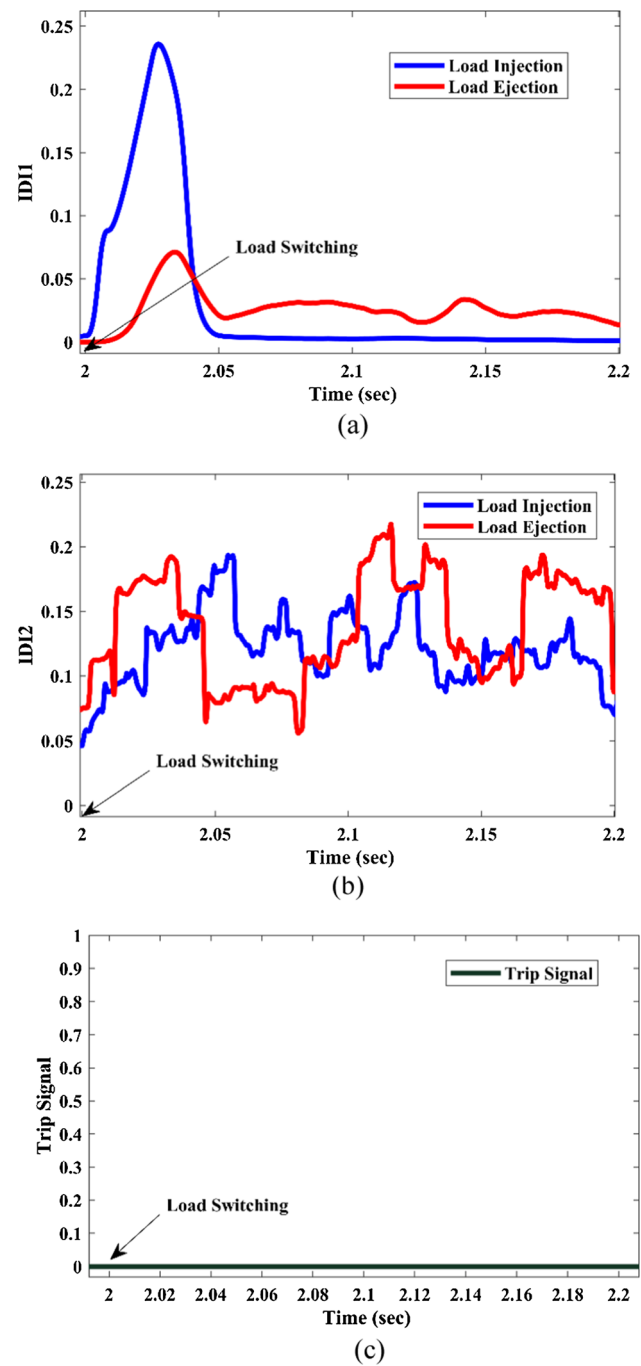

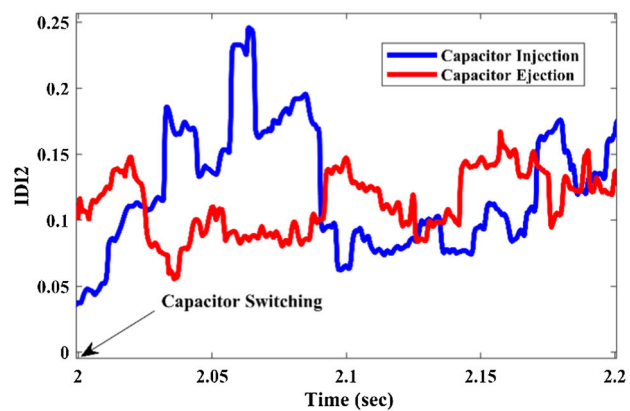**Fig. 5** Load switching response **a** IDI_1 versus time **b** IDI_2 **c** trip signal versus time

case is shown in Fig. 10a. When a heavy load with capacity (22.5 MW and 3.4 MVAR) is ejected from the test system at $t = 2$ s. In this event, the voltage is higher than the rated voltage and is known as a voltage swell. The response to this event is represented in Fig . 10b. From Fig. 10c–d, the magnitude

of IDI_1 and IDI_2 in both cases (injected and ejection) is less than the threshold value (0.9). Therefore, the proposed logic-initiated trip signal is zero as shown in Fig. 10e. Therefore, the power quality (sag and swell) of the distribution network does not affect the proposed mixed scheme.
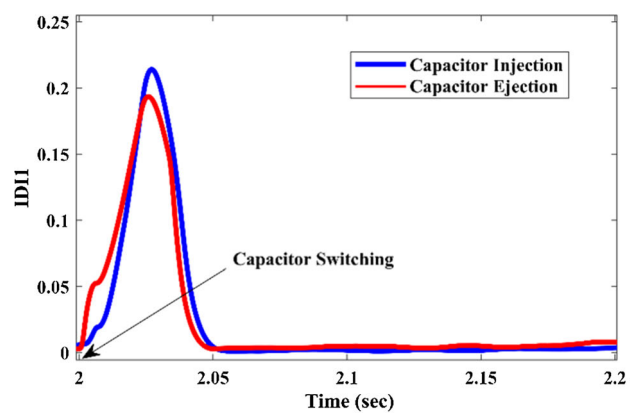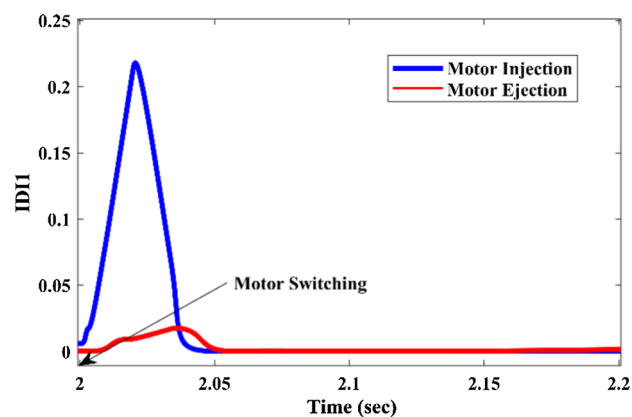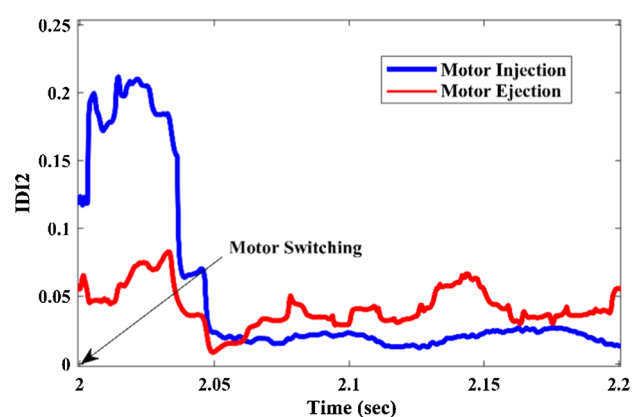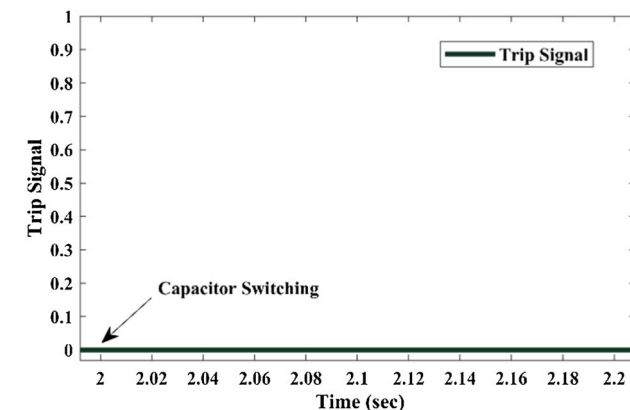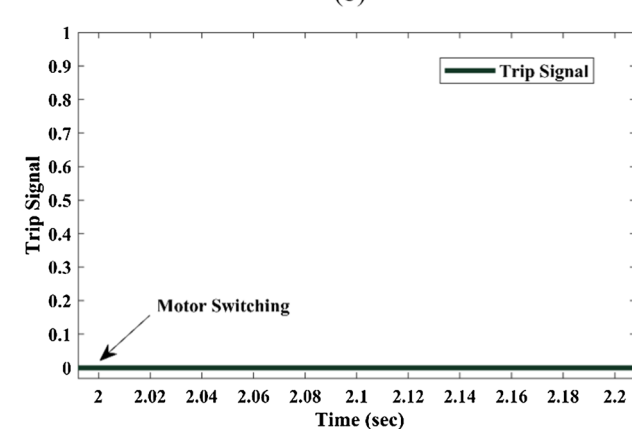
Fig. 6 Capacitor switching response **a** IDI_1 versus time **b** IDI_2 versus time **c** trip signal versus time

Fig. 7 Motor switching response **a** IDI_1 versus time **b** IDI_2 versus time **c** trip signal versus time

5 Comparative analysis and discussion

The proposed approach is tested on a power network with synchronous and wind power DG units in various scenarios of islanding and non-islanding cases. According to the above discussion, the proposed methodology easily distinguishes between islanding and non-islanding conditions for every kind of DG. In this section, a comparative analysis

of the proposed technique with other existing methods is presented in Table 3 which reflects the betterment of the proposed scheme over the existing schemes—be it NDZ, complexity, threshold setting, power quality issue, etc. A comparison of the proposed scheme with a [22] (PAOPSV) is represented in Fig. 11a–b. When the proposed method operated at zero power mismatch, islanding is detected within

Table 3 Comparison of several islanding detection schemes

Islanding detection algorithms	Detection Time	NDZ	Complexity and Cost	Threshold Setting	PQ Issue	NLL	LLLG fault R_f = 0.01Ω	System
Active ROCOF [19]	200 ms	Near zero	Less	Difficult	Yes	–	–	Wind power DG
FHO [20]	1.3 s	– 11 to 9%	Less	Difficult	Yes	–	–	PV and synchronous DG
MPPT Injection [21]	200–300 ms	Low	Less	Moderate	Yes	–	–	PV and synchronous DG
PAOPSV [22]	100 ms	Zero	Medium	Moderate	Yes	–	×	synchronous DG
Multi-LSTM [23]	50 ms	Low	More	Difficult	Yes	–	–	PV and synchronous DG
ROCPSI/ROCNSI [24]	NA	Low	Medium	Difficult	Yes	–	×	PV and synchronous DG
RT-CWT [25]	160 ms	Near zero	Medium	Moderate	Yes	–	×	PV, wind power and synchronous DG
IM [26]	200 ms	Near zero	More	Difficult	Yes	–	–	PV based DG
ROCOV and PIIS [27]	300 ms	zero	More	Moderate	No	–	×	Wind power and synchronous DG
ROCOP-TV [28]	8.2 ms	–	Medium	Difficult	No	–	–	PV based DG
Fuzzy classifier and Reactive power (PV, Load, Grid) [13]	65.2 ms	Zero	Medium	Moderated	No	–	–	PV based DG
Proposed method	20 ms	Zero	Less	Easy	No	√	√	Wind turbine and synchronous DG

$\sqrt{}$ = Verified, $\times$ = Invalid,—= Not consider, NLL = Nonlinear load

20 ms, which is faster than the existing method [22]. However, the previous method [22] detects islanding in 100 ms. The rate of change of power (ROCOP) based on the terminal voltage (TV) (ROCOP-TV) [28] scheme accurately detects the islanding for the photovoltaic (PV) inverter-based microgrids. The ROCOP-TV method is fast and distinguishes between islanding and regular grid faults. However, nonlinear load switching was not considered during the evaluation and NDZ value is not provided. Further, another rate of change of superimposed impedance (ROCSI)-based scheme has a non-detection zone of ± 0.1 to ± 0.5% [29]. Also, this method finds limitations in distinguishing the islanding event (IE) from the non-islanding event (NIE) for LLLG faults with fault resistance Rf = 0.01Ω created in the test network at t

= 2 s, as shown in Fig. 12. Moreover, the technique of [29] was only tested for inverter-based microgrids. However, the proposed scheme successfully distinguishes IEs from NIEs with zero NDZ and it works well for synchronous and wind power-based microgrids.
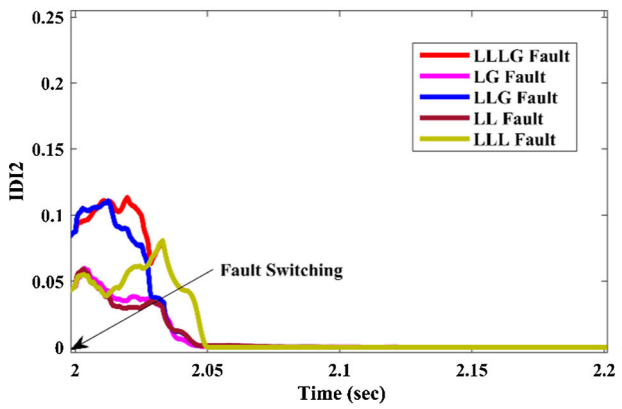
6 Conclusion

In this article, a new mixed islanding technique is proposed to overcome the issue of unintentional islanding. This scheme successfully distinguishes between islanding and non-islanding conditions at zero power mismatch and hence avoids unwanted tripping. The operation of the proposed
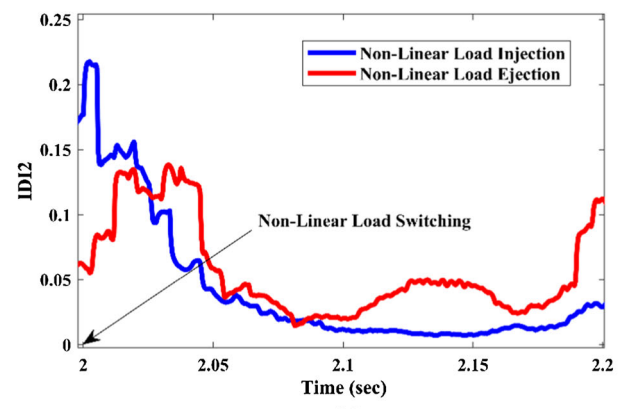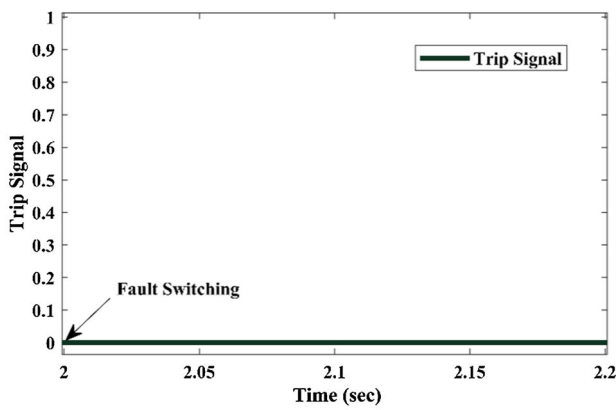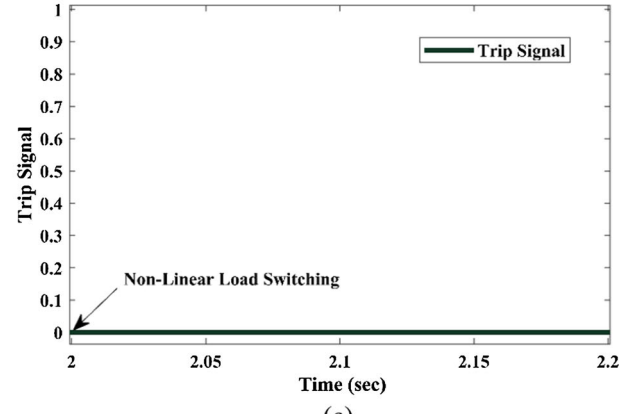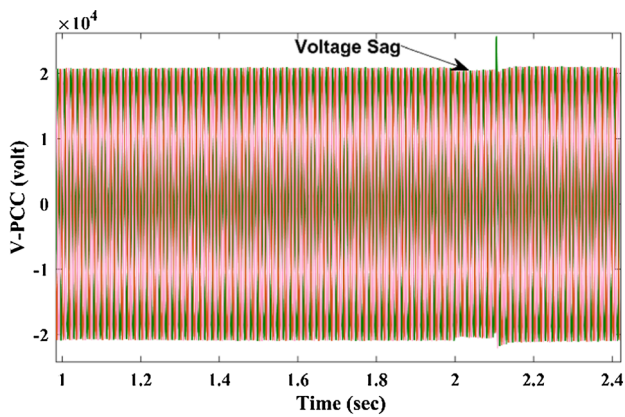
(a)

(b)
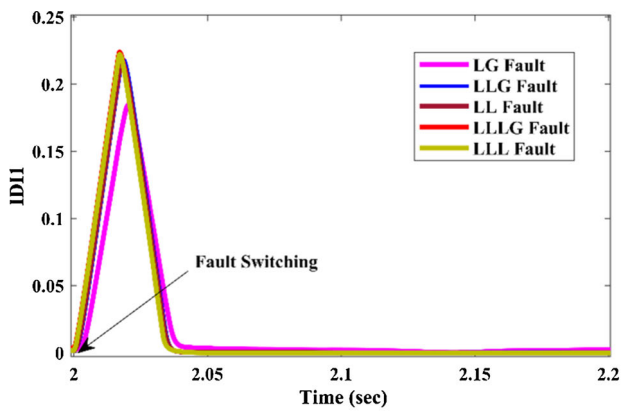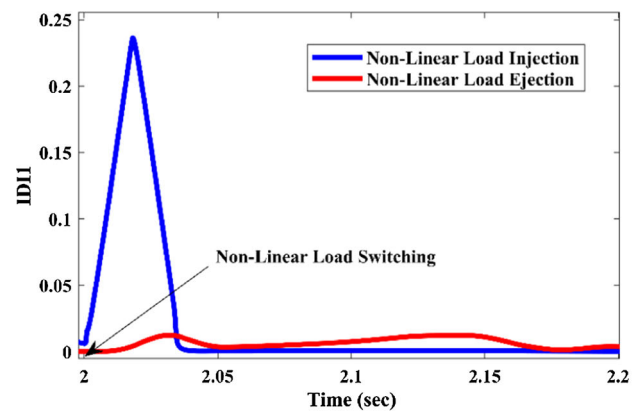
(c)

Fig. 8 Fault switching response **a** IDI$_1$ **b** IDI$_2$ **c** trip signal

(a)

(b)

(c)

Fig. 9 Nonlinear load switching response **a** IDI$_1$ **b** IDI$_2$ **c** trip signal

(a)

(b)

(c)

(d)

(e)
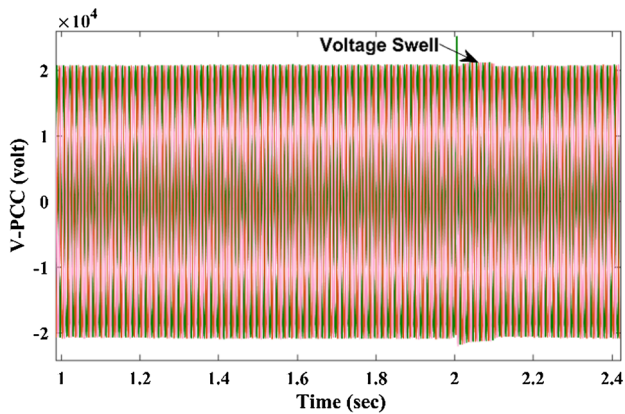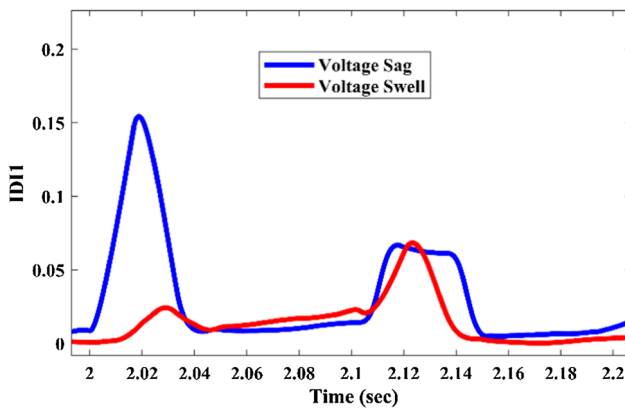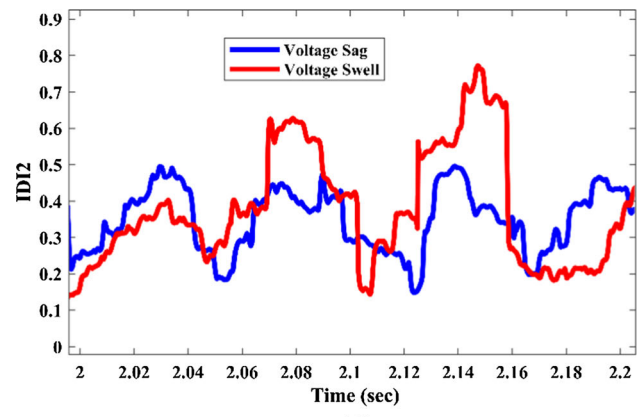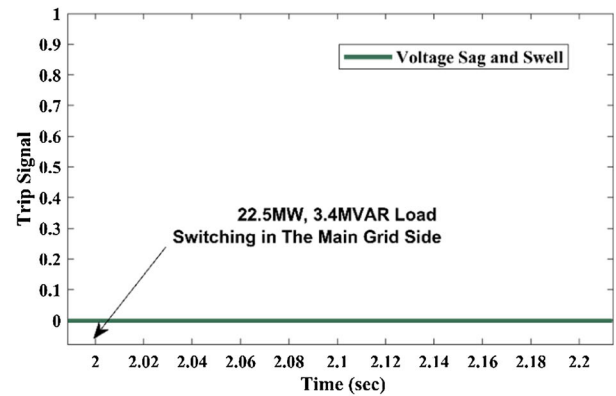
Fig. 10 continued

Fig. 10 **a** Voltage sag at PCC versus time **b** voltage swell at PCC versus time **c** IDI_1 **d** IDI_2 **e** trip signal

scheme works accurately with various islanding and non-islanding events such as load switching, capacitor switching, nonlinear switching, asynchronous motor switching, and fault switching. According to the simulation results, this technique can detect islanding quickly and correctly in 20 ms. The proposed method does not degrade power quality and is simple to implement with low operating costs. This algorithm detects islanding in less than 2 s and adheres to the IEEE 1547 standard. A comparative analysis is also conducted, and the results are believed to be significantly superior. The advice for future work is observed. In this study, only wind power and synchronous-based DG are considered, so an islanding scheme must be developed to extend the results of this paper and work effectively for solar and fuel cell DG systems.
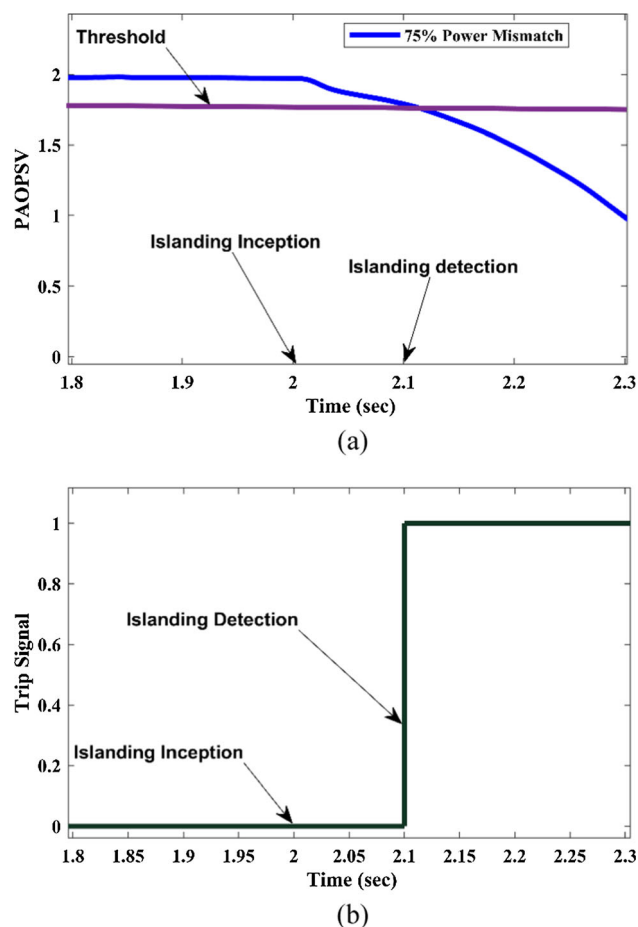
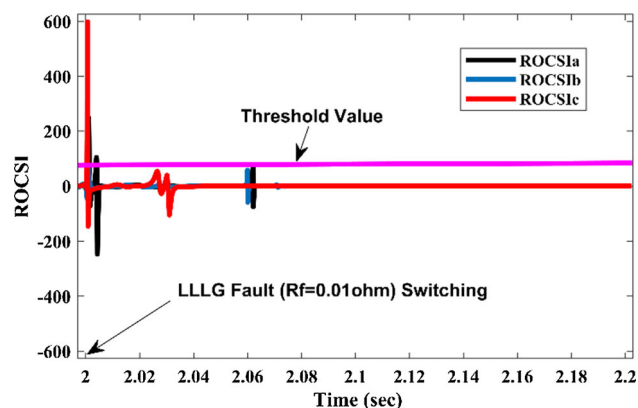Fig. 11 Zero power mismatch islanding condition **a** PAOPSV **b** Trip signal

Fig. 12 The magnitude of ROCSI for the LLLG fault switching with fault resistance $R_f = 0.01\Omega$

Author contributions A. Indradeo Pratap Bharti was involved in conceptualization, methodology, software, writing—original draft. B. Navneet Kumar Singh helped in supervision, writing—review & editing. C. Om Hari Gupta and Ashish Kumar Singh contributed to writing—review & editing.

Declarations

Conflict of interests The authors declare no competing interests.

References

1. IEEE Standard (2018) IEEE standard for Interconnection and interoperability of distributed energy resources with associated electric power systems interfaces, IEEE Standard, pp 1547–2018
2. Reddy CR, Goud BS, Reddy BN, Pratyusha M, Vijay Kumar CV, Rekha R (2020) Review of Islanding Detection Parameters in Smart Grids. In: 2020 8th international conference on smart grid (icSmartGrid), Paris, France
3. Bharti IP, Singh NK, Gupta OH, Singh AK (2021) Developments in islanding detection and its comparison: a comprehensive review. In: 8th IEEE Uttar Pradesh section international conference on electrical, electronics and computer engineering (UPCON-2021).
4. Prudvi Raj P (2023) Islanding detection of IEEE 13 bus system based on sequence components. Int Trans Electric Eng Comput Sci 2:7
5. Rami Reddy C, Harinadha Reddy K (2018) An efficient passive islanding detection method for integrated DG system with zero NDZ. Int J Renew Energy Res 8:4
6. Kumar, M., Kumar, J (2023) Islanding event detection technique based on the change in apparent power in microgrid environment. Electric Eng 105:16
7. Rami Reddy C, Harinadha Reddy K, Karimulla S, Suneel Babu J, Praveen Kumar B, Naveen G (2018) A novel passive approach for islanding detection of integrated DG system under zero power imbalance. Int J Pure Appl Math 120(06):4059–4077
8. Barkat F, Cheknane A, Guerrero JM, Lashab A, Istrate M, Gavrilas M, Motas JG, Banu IV (2023) Review, analysis, and performance evaluation of the most common four active methods for islanding detection in grid-connected photovoltaic systems. Electric Power Syst Res 214:36
9. Rostami A, Jalilian A, Hagh MT, Muttaqi KM, Olamaei J (2019) Islanding detection of distributed generation based on rate of change of exciter voltage with circuit breaker switching strategy. IEEE Trans 55:9
10. Bejmert D, Sidhu TS (2014) Investigation into islanding detection with capacitor insertion-based method. IEEE Trans. Power Del
11. Zamani R, Golshan MEH, Alhelou HH, Hatziargyriou N (2019) A novel hybrid islanding detection method using dynamic characteristics of synchronous generator and signal processing technique. Electr Power Syst Res 175:9

12. Narayanan K, Siddiqui SA, Fozdar M (2017) Hybrid islanding detection method and priority-based load shedding for distribution networks in the presence of DG units. IET Gener Transm Distrib 11(3):586–595

13. Elshrief YA, Asham AD, Bouallegue B, Ahmed A, Helmi DH, Abozalam BA, Abd-Elhaleem S (2022) An innovative hybrid method for islanding detection using fuzzy classifier for different circumstances including NDZ. J Radiat Res Appl Sci 15:14

14. Kumar P, Kumar V, Tyagi B (2021) A novel islanding detection technique based on event index value for reconfigurable microgrid. IEEE Trans Ind Appl 57(4):3451–3462

15. Kermany SD, Joorabian M, Deilami S, Masoum MA (2017) Hybrid islanding detection in microgrid with multiple connection points to smart grids using the fuzzy-neural network. IEEE Trans Power Syst 32(4):2640–2651

16. Lázár E, Etz R, Petreuş D, Pătărău T, Ciocan I (2015) SCADA development for an islanded microgrid. In: IEEE 21st international symposium for design and technology in electronic packaging, pp 147–150

17. Krishnan MG, Ashok S (2012) Implementation of recursive DFT algorithm for phasor measurement unit (PMU). In: 2012 IEEE international conference on engineering education: innovative practices and future trends (AICERA), Kottayam, India, 2012, pp. 1–5. https://doi.org/10.1109/AICERA.2012.6306751.

18. Jayachandran M, Reddy CR, Padmanaban S, Milyani AH (2021) Operational planning steps in smart electric power delivery system. Sci Rep 11:21

19. Gupta P, Bhatia RS, Jain DK (2017) Active ROCOF relay for islanding detection. IEEE Trans Power Deliv 32(1):420–429

20. Bakhshi M, Noroozian R, Gharehpetian GB (2018) Novel islanding detection method for multiple DGs based on forced Helmholtz oscillator. IEEE Trans on Smart Grid 9(6):6448–6460

21. Bakhshi-Jafarabadi R, Sadeh J, Popov M (2021) Maximum power point tracking injection method for islanding detection of grid-connected photovoltaic systems in microgrid. IEEE Trans Power Deliv 36(1):12

22. Shafique N, Raza S, Bibi S, Farhan M, Riaz M (2022) A simplified passive islanding detection technique based on susceptible power indices with zero NDZ. Elsevier Ain Shams Eng J 13

23. Kaymaz Ozcanl A, Baysal M (2022) A novel multi-LSTM based deep learning method for islanding detection in the microgrid. Elsevier Electric Power Syst Res 202:12

24. Sareen K, Bhalja BR, Maheshwari RP (2016) Universal islanding detection technique based on the rate of change of sequence components of currents for distributed generations. IET Renew Power Gener 10(2):228–237

25. Cavalcante Paiva S, Lúcio de Araujo Ribeiro R, Keuton Alves D, Bezerra Costa F, de Oliveira Alves Rocha T (2020) A wavelet-based hybrid islanding detection system applied for distributed generators interconnected to AC microgrids. Elsevier Electrical Power Energy Syst 121:10

26. Bei T (2017) Accurate active islanding detection method for grid-tied inverters in a distributed generation. IET Renew Power Gener 11(13):1633–1639

27. Rostami A, Jalilian A, Zabihi S, Olamaei J, Pouresmaeil E (2020) Islanding detection of distributed generation based on parallel inductive impedance switching. IEEE Syst J 14:11

28. Elshrief YA, Helmi DH, Abd-Elhaleem S, Ahmed Abozalam B, Asham AD (2021) Fast and accurate islanding detection technique for microgrid connected to a photovoltaic system. J Radiat Res Appl Sci 14:11

29. Tadikonda N, Kumar J, Mahanty RN (2022) A technique for detection of islanding in a microgrid based on the rate of change of superimposed impedance. Electric Power Syst Res 206:18